Journal of Materials Chemistry A

Accepted Manuscript

This is an *Accepted Manuscript*, which has been through the Royal Society of Chemistry peer review process and has been accepted for publication.

Accepted Manuscripts are published online shortly after acceptance, before technical editing, formatting and proof reading. Using this free service, authors can make their results available to the community, in citable form, before we publish the edited article. We will replace this *Accepted Manuscript* with the edited and formatted *Advance Article* as soon as it is available.

You can find more information about *Accepted Manuscripts* in the Information for Authors.

Please note that technical editing may introduce minor changes to the text and/or graphics, which may alter content. The journal's standard Terms & Conditions and the Ethical guidelines still apply. In no event shall the Royal Society of Chemistry be held responsible for any errors or omissions in this *Accepted Manuscript* or any consequences arising from the use of any information it contains.

ROYAL SOCIETY OF CHEMISTRY

www.rsc.org/materialsA

Cyclodextrin-based supramolecular polymeric nanoparticles for next generation gas separation membranes

Shereen Tan,[‡a] Qiang Fu,[‡a,b] Joel. M. P. Scofield,[a,b] Jinguk Kim,[a,b] Paul A. Gurr,[a] Katharina Ladewig,[a] Anton Blencowe,[c,d] Greg. G. Qiao[*a,b]

[a] Polymer Science Group, Department of Chemical and Biomolecular Engineering, The University of Melbourne, Parkville, VIC 3010, Australia.
[b] Cooperative Research Centre for Greenhouse Gas Technologies, The University of Melbourne, Parkville, VIC 3010, Australia.
[c] Mawson Institute, Division of ITEE, The University of South Australia, Mawson Lakes, SA 5095, Australia.
[d] School of Pharmacy and Medical Sciences, Division of Health Sciences, The University of South Australia, Adelaide, SA 5001, Australia.
*e-mail: gregghq@unimelb.edu.au
‡ These authors contributed equally.

TOC

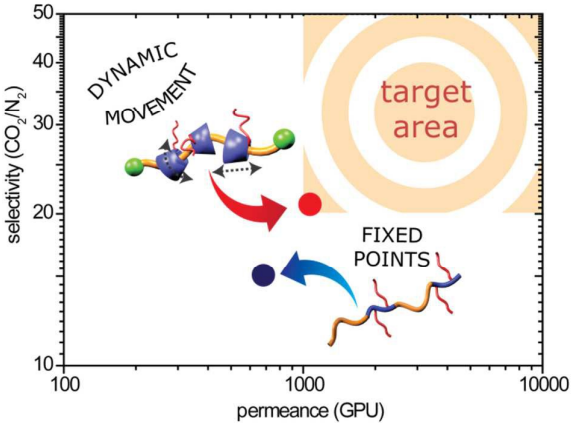

Cyclodextrin-based supramolecular assemblies derived from poly(dimethylsiloxane) functionalized polyrotaxanes are for the first time used as soft nanoparticle additives for the selective layer of thin film composite membranes. The dynamic nature of the conjugated poly(dimethylsiloxane) chains provides the corresponding films with outstanding gas transport characteristics, which allow low percentages of additives to be incorporated whilst maintaining performance targets set by industry standards.

Journal of Materials Chemistry A Accepted Manuscript

Abstract

Cyclodextrin-based supramolecular assemblies derived from poly(dimethylsiloxane) (PDMS) functionalized polyrotaxanes (PRXs) were self-assembled into core-shell morphologies and used as soft nanoparticle (SNP) additives in the selective layer of thin film composite (TFC) membranes for the first time. Various weight percentages (wt%) of the PRX SNP additives were combined with Pebax® 2533 to form the selective layer and the gas transport properties of the TFC membranes were studied in detail. Increasing the amount of PRX SNP additives lead to a significant increase in CO_2 permeance of the membranes, with only a slight decrease in the CO_2/N_2 selectivity, which was attributed to the dynamic nature (i.e., translational and rotational freedom) of the conjugated PDMS chains on the PRXs. In comparison, the performance of membranes prepared using a conventional analogue with fixed PDMS chains was inferior. The excellent gas transport properties observed for membranes are attributed to the novel self-assembly process of the dynamic PRX SNP additives; the sliding nature of the conjugated PDMS chains allow for increased exposure of the CO_2-phillic PEG backbone and increased size of the hydrophobic core leading to improved membrane selectivity and permeability. The effect of varying operating conditions (feed pressure and temperature) was also investigated and compared between the dynamic and fixed additive systems. Interesting trends were observed with the dynamic PRX system which diverges from conventional systems. This study opens up new avenues for CD-based supramolecular chemistry in the field of membrane technologies for gas separation.

1. Introduction

Industrialisation has led to a substantial rise in global carbon dioxide (CO_2) levels which have had, and continue to have a detrimental impact on the environment. Thus, a significant world-wide effort is being directed to reduce carbon emissions.[1-3] The separation of CO_2 from flue gas emissions from industrial power plants followed by geo-sequestration has received widespread interest as this process could potentially lead to a 40 % reduction of CO_2 emissions world-wide.[1] The use of membrane technologies for CO_2 separation is of significant commercial interest due to their low capital costs and

Journal of Materials Chemistry A Accepted Manuscript

low carbon footprint when compared to traditional methods such as chemical adsorption by amine-based solutions.[2, 4]

Extensive research has focused on developing different classes of membrane materials which display excellent gas separation performance to further reduce the cost of membrane technology. This includes inorganic zeolite based membranes which generally observe high gas separation performance due to their intrinsic porosity and ability to interact preferentially with CO_2.[5, 6] Additionally, a new class of membranes termed polymers of intrinsic microporosity (PIM) has also been shown to observe higher gas separation performance when compared to common polymeric polymers as they have a rigid ladder-like conformation creating larger free-volume elements.[7] Although both these dense materials observe high gas selectivity and permeability, it is often operationally difficulty to form the membranes into spiral sheets or hollow fibre modules, which are essential for industry. Thus, the fabrication of multi-layer polymeric membranes in the form of thin film composites (TFCs) is commercially more desirable as they can be implemented into spiral and hollow fibre modules while achieving higher fluxes, and potentially reducing the consumption of expensive polymeric materials.[8-10] Polymeric membranes exhibiting both high selectivity and high permeance are highly sought after. However, current polymeric materials generally exhibit a low permeance with high selectivity.[1, 3] One common method used to enhance the permeation rate is through the introduction of inorganic or organic-inorganic nanoparticles.[3, 11, 12] Although the resulting mixed matrix membranes (MMM) display preferential gas transport through the particulates, it is often difficult to obtain a defect-free interface between the organic and inorganic phases. This draw-back often affects membrane integrity and reduces membrane separation performance. Furthermore, it is often difficult to fabricate particles in a size range which does not exceed the selective layer thickness (generally < 400 nm) in TFC membrane systems.[1, 3, 11, 13, 14] Through the utilization of organic based soft nanoparticles (SNPs), the concept of MMMs can also be replicated[13, 15, 16] while additionally offering greater tailorability. This allows for better compatibility between the polymer matrix and additives, resulting in greater control of the membrane's gas separation performance. For example, the incorporation of CO_2-philic ethylene glycol (EG) units is often desirable as high CO_2 solubility is observed.[17] However, conventionally this cannot be achieved due to the high degree of crystallisation of poly(ethylene glycol) (PEG) resulting in poor gas

Journal of Materials Chemistry A Accepted Manuscript

transport properties.[18] Conversely, through the use of SNPs, a high degree of EG units can easily be incorporated by the addition of rigid spacers between the EG blocks or by adopting a hyperbranched configuration.[13, 15, 16] The ability to tailor the composition of the additives down to a molecular level also allows greater control of additive size and morphology. For example, block *co*-polymers consisting of PEG and poly(dimethylsiloxane) (PDMS) of varying lengths can self-assemble into multi-core nanoparticles, which leads to changes in the gas transport properties.[19] These studies have provided a basis for understanding the relationship between SNP structure and their corresponding gas transport properties, thus providing a better handle in controlling permeance and selectivity.

The application of cyclodextrin (CD)-based supramolecular chemistry can be used as a novel route towards the fabrication of SNPs which exhibit sophisticated and dynamic morphologies. Generally composed of six-to-eight D-glucose units, CDs are able to form tight, yet reversible complexes with various guest molecules and polymeric chains.[20] Polyrotaxanes (PRXs) were one of the first supramolecular constructs to be fabricated using this feature and consist of α-CD moieties threaded onto a PEG-based backbone.[21] Through the addition of bulky-end groups on both ends of the backbone, the CDs moieties are able to retain translational and rotational freedom about the axis without complete disassociation of the complex.[22-24] This novel feature provides PRXs with unique and interesting properties that can be utilized to fabricate sophisticated architectures[25, 26] and functional materials with various applications, including highly elastic scratch resistant films,[27, 28] nanocoatings for bio-nanotechnology[29] and drug-polymer conjugates.[30]

By utilising the dynamic features of PRXs, we report for the first time, SNPs derived from PDMS conjugated CD/PEG-based PRXs. The mobility of the PDMS conjugated CDs along the PEG axel and the hydrophobicity of the PDMS chains results in the PRXs self-assembling into core-shell particles (i.e., SNPs). Subsequently, the supramolecular SNPs were physically blended with Pebax® 2533 to afford the selective layer of TFC membranes. When compared to membranes casted with SNPs comprised of fixed PDMS chains, the membranes casted with dynamic PRX based SNPs observed a 30 % increase in CO_2 selectivity while using 50 % less additives. The increase in gas performance when PRX based SNPs are used is attributed to the novel self-assembly process where

Journal of Materials Chemistry A Accepted Manuscript

the sliding nature of the conjugated PDMS chains allow for increased exposure of the CO_2-phillic PEG backbone of the PRXs and increased size of the hydrophobic core leading to improved membrane selectivity and permeability. Interesting trends were also observed between dynamic and fixed systems when the operating conditions (i.e., feed pressure and temperature) were varied. The ability of these materials to obtain gas transport properties within performance targets set by industry at significantly lower additive concentrations when compared to the current reports,[13, 19] opens up new avenues for CD-based supramolecular chemistry in the field of membrane technology for CO_2 separation.

2. Experimental

2.1. Materials

Trimesoyl chloride (TMC, 98%), anhydrous *t*-butanol (*t*-BuOH, 99.5%), *α*-cyclodextrin (*α*-CD, 98%), poly(ethylene glycol) (MALDI-TOF MS: M_n = 11,100 Da and M_n = 400 Da), *N,N'*-Dicyclohexylcarbodiimide (DCC, 99%), 5-hexynoic acid (97%), tetra-*n*-butylammonium hydrogen sulphate (TBAHS, 99+%), 3-chloro-1-propanol (98%), copper (I) bromide (Cu(I)Br, purum), *N,N,N',N'',N''*-pentamethyldiethylenetriamine (PMDETA, 99%), ethylenediaminetetraacetic acid (EDTA, 99%) and succinic anhydride (>99%) were purchased from Sigma-Aldrich and used without further purification. 9-Anthracenecarboxylic acid (purum, Fluka), thionyl chloride (Merck), anhydrous magnesium sulphate ($MgSO_4$, Merck), , 4-(dimethylamino)pyridine (DMAP, 99%, Fluka), anhydrous dimethyl sulfoxide (DMSO, >99%, Fluka), pyridine (AR grade, >99.5 %, Scharlau), anhydrous *N,N*-dimethylformamide (DMF, 99.8%, Acros Organics) and *N*-(3-(dimethylamino)propyl)-*N*-ethylcarbodiimide hydrochloride (EDCI, 98+%, Acros Organics) were all used as received. Aminopropyl terminated polydimethylsiloxane (NH_2-PDMS-NH_2, M_n = 5,000 Da) and α-hydroxyethoxypropyl-ω-butyl terminated polydimethylsiloxane (PDMS-OH, M_w = 1,000 Da) were both obtained from Gelest Inc. and used as received. Diethyl ether (DEE, AR), dichloromethane (DCM, AR), methanol (MeOH, AR), isopropanol (IPA, AR), *n*-butanol (n-BuOH, AR), hexane (AR), ethyl acetate (AR) and sodium azide (99%) were obtained from Chem-Supply and used as received. Anhydrous triethylamine (TEA) and tetrahydrofuran (THF) were obtained by distillation under argon from CaH_2 and sodium benzophenone ketyl, respectively.

Journal of Materials Chemistry A Accepted Manuscript

Deuterated dimethylsulfoxide (d_6-DMSO) and chloroform ($CDCl_3$) were obtained from Cambridge Isotope Laboratories and used as received. SnakeSkin dialysis tubing (MWCO = 7,000 Da) was obtained from Thermo Scientific. Pebax® 2533 was obtained from Arkema and polyacrylonitrile (PAN) microporous support was purchased from SolSep BV.

2.2 Instrumentation

Proton nuclear magnetic resonance (^{1}H NMR) spectroscopy was conducted on a Varian Unity 400 MHz spectrometer operating at 400 MHz, using the deuterated solvent as reference and at a sample concentration of *ca.* 20 mg·mL^{-1}. Dynamic light scattering (DLS) measurements were performed on a Wyatt DynaPro NanoStar fitted with a 120 mW Ga-As laser operating at 658 nm; 100 mW was delivered to the sample cell. Analysis was performed at an angle of 90° and at constant temperatures of either 25 ± 0.01 or 40 ± 0.01 °C. X-ray diffraction (XRD) patterns of the samples were recorded on a Bruker D8 Advance instrument with Cu Kα radiation (40 kV, 40 mA) and a nickel filter, and the samples were exposed at a scanning rate of 2θ = 0.020 °·s^{-1} in the range of 3-70°. Scanning electron microscopy (SEM) images were acquired using FEI Quanta 200 ESEM. Samples were pre-coated with gold using Dynavac Mini Sputter Coater prior to imaging.

2.3 Synthesis of soft polymeric nanoparticles

Synthesis of carboxylic acid terminated PDMS (PDMS-COOH)

α-Hydroxyethoxypropyl-*ω*-butyl terminated PDMS (1.0 mL, 0.001 mmol, 1 equiv.), succinic anhydride (0.15 mg, 0.002 mmol, 1.5 equiv.), pyridine (0.12 mL, 0.002 mmol, 1.5 equiv.) and DMAP (0.01 mg, 0.0001 mmol, 0.1 equiv.) were dissolved in distilled DCM (5 mL) under N_2 atmosphere and stirred continuously at 60 °C for 16 hours. The crude product was concentrated *in vacuo* (20 mbar, 40 °C), redissolved in DCM (2mL) and precipitated into hexane (20 mL) before being dried *in vacuo* (20 mbar) to afford the product as a viscous liquid, 841 mg (74 %). ^{1}H NMR (400 MHz, $CDCl_3$): δ_H 0.04-0.08 (*m*, OSi(C$\boldsymbol{H_3}$)$_2$ repeat unit), 0.50-0.56 (*m*, 4H, C$\boldsymbol{H_2}$Si & SiC$\boldsymbol{H_2}$), 0.88 (*m*, 3H, CH_2C$\boldsymbol{H_3}$), 1.26-1.35 (*m*, 4H, CH_3C$\boldsymbol{H_2}$C$\boldsymbol{H_2}$$CH_2$), 1.61 (*m*, 2H, Si$CH_2C\boldsymbol{H_2}$$CH_2$O), 2.67 (*t*, 4H, *J* = 3.2 Hz, O=CC$\boldsymbol{H_2}$C$\boldsymbol{H_2}$COOH), 3.42 (*t*, 2H, *J* = 7.2 Hz, CH_2 CH_2C$\boldsymbol{H_2}$O), 3.63 (*t*, 2H, *J* = 4.8 Hz, OC$\boldsymbol{H_2}$$CH_2$O), 4.25 (*t*, 2H, *J* = 4.8 Hz OCH_2C$\boldsymbol{H_2}$OC=O) ppm. MALDI-ToF MS: M_n shift = 100 *m*/*z*.

Journal of Materials Chemistry A Accepted Manuscript

*Synthesis of PEG$_{10K}$-α-CD polyrotaxane **P0***

The PEG-based polyrotaxane **P0** was synthesized according to the literature.[28, 29] ^{1}H NMR (400 MHz, d_6-DMSO): δ_H 1.79 (*quin*, 2H, *J* = 7.2 Hz, $CH_2C\boldsymbol{H_2}CH_2$), 2.20 (*dt*, 2H, *J* = 2.8 & 7.2 Hz, =$CC\boldsymbol{H_2}CH_2$), 2.34-2.41 (*m*, 4H, $COC\boldsymbol{H_2}CH_2$, $CH_2C\boldsymbol{H_2}O$), 3.29-3.69 (*m*, 2H, $C\boldsymbol{H_2}O$), 4.11-4.14 (*m*, 4H, $C\boldsymbol{H_2}C\boldsymbol{H_2}O$), 4.80 (*d*, 6H, $OC\boldsymbol{H}CH_2$ of α-CD), 5.38-5.64 (*s*, 12H, $CH_2O\boldsymbol{H}$ of α-CD), 7.61 (*q*, 4H, Ar***H***), 7.90 (*s*, 1H, =C***H***N), 8.01 (*d*, 2H, Ar***H***), 8.20 (*d*, 2H, Ar***H***), 8.80 (*s*, 1H, Ar***H***) ppm.

*Synthesis of PDMS functionalized polyrotaxanes **P1***

Polyrotaxane **P0** (100 mg, 0.007 mmol, 1 equiv.), PDMS-COOH (378 mg, 0.38 mmol, 54 equiv.), EDCI (40.3 mg, 0.21 mmol, 30 equiv.) and DMAP (2.6 mg, 0.021 mmol, 3 equiv.) were dissolved in anhydrous DMSO (1 mL) and stirred at 60 °C for 4 days in a sealed flask. The crude reaction mixture was then concentrated *in vacuo* (0.1 mbar, 50 °C), redissolved in DMF (1.5 mL), precipitated into DEE (15 mL) and collected by centrifugation before being dried *in vacuo* (0.1 mbar, 60 °C) to afford **P1** as a slight yellow powder, 210 mg (54 %). ^{1}H NMR (400 MHz, d_6-DMSO): δ_H -0.1-0.06 (*m*, $Si(C\boldsymbol{H_3})_2O$), 0.40-0.53 (*m*, 4H, $C\boldsymbol{H_2}Si$ & $SiC\boldsymbol{H_2}$), 0.74-0.87 (m, 3H, $CH_2C\boldsymbol{H_3}$), 1.27-1.31 (m, 4H, $CH_3C\boldsymbol{H_2}C\boldsymbol{H_2}CH_2$), 1.47-1.54 (m, 2H, $SiCH_2C\boldsymbol{H_2}CH_2O$), 2.41 (*m*, 4H, $COC\boldsymbol{H_2}CH_2$, $CH_2C\boldsymbol{H_2}C{=}O$), 3.29- 3.69 (*m*, 2H, $C\boldsymbol{H_2}O$), 4.11-4.14 (*m*, 4H, $C\boldsymbol{H_2}C\boldsymbol{H_2}O$), 4.80 (*m*, 6H, $OC\boldsymbol{H}CH_2$ of α-CD), 5.38-5.64 (*s*, 12H, $CH_2O\boldsymbol{H}$ of α-CD), 7.61 (*m*, 4H, Ar***H***), 7.90 (*s*, 1H, =C***H***N), 8.01 (*d*, 2H, Ar***H***), 8.20 (*d*, 2H, Ar***H***), 8.80 (*s*, 1H, Ar***H***) ppm.

*Synthesis of PDMS functionalized poly(ethylene glycol-co-glycidol) (PEG-g-PDMS) **P2***

The synthesis of PDMS functionalised poly(ethylene glycol-*co*-glycidol) was adapted from the literature,[31] and involved three steps: (i) the copolymerization of ethylene oxide (EO) and 2,3-epoxypropyl-1-ethoxyethyl ether protected glycidol (EEGE) to prepare the copolymer P(EG-*co*-EEGE); (ii) hydrolysis of the copolymer to form poly(ethylene glycol-*co*-glycidol) (P(EG-*co*-Gly)) and (iii) the partial esterification of P(EO-*co*-Gly) with PDMS-COOH.

(i) *Synthesis of copolymer P(EG-co-EEGE)*

Copolymerization was conducted according to the literature under the help of A. Prof. Wang (Fudan University, China). ^{1}H NMR (400 MHz, $CDCl_3$) δ_H: 1.20-1.15 (*m*, 3H,

Journal of Materials Chemistry A Accepted Manuscript

C***H₃***CH₂O), 1.30-1.22 (*m*, 3H, O(C***H₃***)CHO), 3.79-3.41 (*m*, 4H, C***H₂***C***H₂***O), 4.74-4.62 (*s*, 1H, O(CH_3)C***H***O-) ppm. GPC-MALLS (DMF) M_n = 22.7 kDa, PDI = 1.08.

(ii) *Synthesis of copolymer P(EG-co-Gly)*

Deprotection of P(EG-co-EEGE) was conducted according to the literature. ^{1}H NMR (400 MHz, $CDCl_3$) δ_H: 3.79-3.41 (*m*, 4H, C***H₂***C***H₂***O) ppm. GPC-MALLS (DMF) M_n = 21.1 kDa, PDI = 1.10.

(iii) *Synthesis of copolymer PEG-g-PDMS **P2***

P(EG-*co*-Gly) (100 mg, 0.005 mmol, 1 equiv.), PDMS-COOH (30 mg, 0.03 mmol, 6 equiv.), EDCI (5.8 mg, 0.03 mmol, 6 equiv.) and DMAP (1.8 mg, 0.02 mmol, 3 equiv.) were dissolved in DCM (2 mL) and stirred at 25 °C for 18 h in a sealed flask. The crude reaction mixture was then precipitated into DEE (20 mL) and collected by centrifugation. The product was dried *in vacuo* (1 mbar, 30 °C) to afford **P2** as a white powder, 81 mg (62 %). ^{1}H NMR (400 MHz, $CDCl_3$) δ_H : 0.04 to 0.08 (*m*, Si(C***H₃***)₂O), 0.05-0.55 (*m,* 2H, SiC***H₂***CH₂), 0.88 (t, *J* = 7.2 Hz, CH₂C***H₃***), 1.21-1.32 (m, 4H, CH₂(C***H₂***)₂CH₃), 1.56-1.64 (m, 2H, OCH₂C***H₂***CH₂), 2.86 (*s*, 4H, O(C***H₂***)₂CO), 3.51 (*s*, 2H, OC***H₂***CH₂), 3.59-3.74 (*m*, 11H, O(C***H₂***)₂O, OC**H₂**C***H***CH₃ and OC***H₂***C*H*C***H₂*** backbone), 4.09-1.45 (*m*, 2H, OCH₂C***H₂***O), 4.21-4.24 (*m*, 2H, CHC***H₂***OC=O), 4.47-4.51 (*m*, 2H, OC***H₂***CH₂) ppm.

2.4 Membrane preparation

A solution of diamino terminated PDMS (NH_2-PDMS-NH_2, 0.80 g, 0.16 mmol) in hexane (20 mL, 4 wt%) was combined with TMC (0.021 g, 0.079 mmol) in hexane (0.525 mL, 4 wt%). The solution was filtered through a 0.45 µm PTFE filter and aliquots of the solution (1.0 mL) were spin coated at 1,000 rpm onto pre-wetted (H_2O) circular PAN substrates (*D* = 4.2 cm) for 15 s. The membranes were dried *in vacuo* (0.1 mbar) overnight and tested for their gas transport properties to ensure that there were no leakages before subsequent coating of the selective layer.

Pebax® 2533 was dissolved in a mixture of IPA:*n*-BuOH (3 : 1 vol%) at 80 °C over 48 h to afford a Pebax® stock solution (2.0 wt%). After cooling to room temperature, different amounts of additives (**P0**, **P1**, **P2**, α-CD or PDMS-OH (M_w = 1,000 Da)) were added (5 - 30 wt% relative to the amount of Pebax® 2533) and stirred at 40 °C for 30 min. IPA:*n*-BuOH is a binary solvent that dissolves Pebax® 2533 and the additives and also does not damage or dissolve the PDMS gutter layer or the micrporous substrate. 1.5

Journal of Materials Chemistry A Accepted Manuscript

mL of the mixture was then spin-coated (1,500 rpm, 20 s) onto the substrate that was pre-coated with the PDMS gutter layer. The TFC membranes were then dried *in vacuo* (0.1 mbar) at 25 °C for 24 h and tested for their gas transport properties using a constant pressure variable volume (CPVV) apparatus (**Scheme 1**).

2.5 Gas permeation experiments

Single gas measurements of thin film composite (TFC) membranes were tested using an in-house built constant pressure variable volume (CPVV) apparatus shown in **Scheme 1**. The TFC membranes were installed in a stainless steel cell and tested for single gases (N_2 and CO_2) under a range of pressures (340 to 1,000 kPa) and temperatures (25, 35 and 45 °C). All data presented in this work was collected from at least three TFC membranes. PAN substrates that were pre-coated with a PDMS gutter layer were also tested to ensure they were defect free using the same gases at a temperature of 35 °C and a pressure of 340 kPa. The flow rate of the single gases was recorded manually with a digital flow meter (Agilent Technologies ADM 2000).

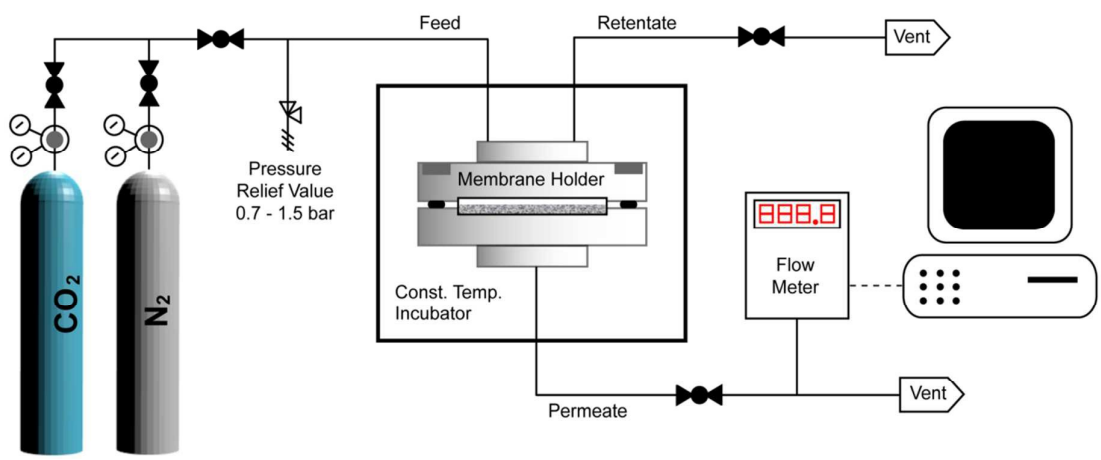

Scheme 1. Schematic diagram of the apparatus used for gas permeation measurements.

2.6 Mass transport theory

The mass transport in non-porous polymeric membranes follows the solution-diffusion mechanism that has been well documented in the literature.[13, 15, 32] The flux (*J*) of a single gas A can be calculated from equation (1):

$$J_A = P_A\left(\frac{\Delta p}{l}\right) \quad (1)$$

Journal of Materials Chemistry A Accepted Manuscript

Where P_A is the permeability of gas A in Barrer, Δp is the pressure difference across the membrane in bar, and l is the membrane thickness in μm.

The membrane permeance is defined as the permeability divided by the membrane thickness and has a unit of GPU. This permeance can also be expressed in terms of a total resistance to flow (R_T) by:

$$J_A = \left(\frac{P_A}{l}\right).\Delta p = \frac{\Delta p}{R_T} \tag{2}$$

In turn, the total resistance (R_T) of permeation through TFC membranes can be expressed as the sum of the resistances from the feed side boundary layer (R_F), the permeate side boundary layer (R_P), the membrane selective layer (R_{SL}), and the gutter layer (R_G) coated on the porous substrate:

$$R_T = R_F + R_P + R_{SL} + R_G \tag{3}$$

The boundary layer resistances (R_F and R_P) arise from concentration gradients that are formed at the surface of the membrane in mixed gas systems. However, such concentration polarization is not possible for single gas permeation. Thus the total resistance to flow is related only to the respective thicknesses of the selective and gutter layers (see **Scheme 2**) and their respective permeability:

$$R_T = R_{SL} + R_G = \frac{l_{SL}}{P_{SL}} + \frac{l_G}{P_G} \tag{4}$$

The resistance to flow through the gutter layer ($R_G = l_G/P_G$) can be determined by measuring the flux through this layer prior to deposition of the selective layer. Equations (2) and (4) can then be used to determine the permeance and permeability through the selective layer, by measuring the flow through the combined TFC membrane. However, it should be noted that the estimation of the permeability is highly dependent on the accuracy in determining the thickness of the selective layer.

The ideal single gas selectivity ($\alpha_{A/B}$) between two gases A and B can be expressed by the following equation:

$$\alpha_{A/B} = \frac{P_A}{P_B} \tag{5}$$

Journal of Materials Chemistry A Accepted Manuscript

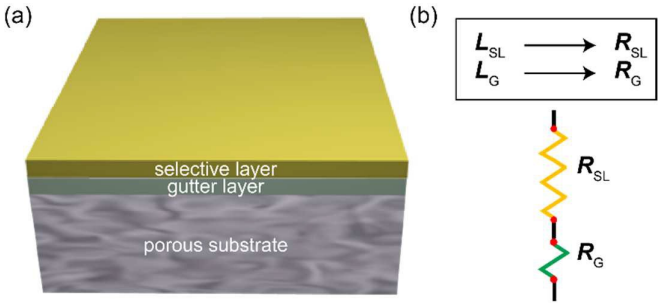

Scheme 2. Graphical illustration of **(a)** the cross-section of a generic TFC membrane and **(b)** the respective analog electrical circuit. Note L_{SL} and L_G are the thickness of the ultra-thin selective layer and the PDMS gutter layer, respectively. R_{SL} and R_G are the resistances of the selective layer and PDMS layer, respectively.

3. Results and Discussion

3.1 Synthesis of PEG-based PRX, P0

The PRX was synthesised by slight modification of methods reported in the literature.[29] Briefly, a polypseudorotaxane was first synthesised by threading α-CD onto a *α,ω*-dialkyne PEG_{10K}. Subsequently, the product was lyophilised prior to end capping *via* copper catalysed azide-alkyne cycloaddition (CuAAC) with an azido-anthracene derivative (**Scheme 3a**, **Scheme S1a**) to afford PRX **P0**. From ^{1}H NMR spectroscopic analysis, the amount of CD per PEG chain (i.e., inclusion ratio) and the end-capping efficiency were determined to be *ca.* 3 CDs and 80 %, respectively (integral ratios of resonances **1** with **a** and **b** and resonances **l** with **1**, respectively, SI, **Fig. S1**). PRX **P0** was self-assembled in an IPA:*n*-BuOH (3: 1 vol%) mixture at 40 °C to obtain SNPs, which were then incorporated into the selective layer of TFC membranes.

3.2 Synthesis of PDMS-functionalised PRX (PRX-*g*-PDMS, P1)

A highly gas permeable PDMS acid derivative was conjugated onto the PRX **P0** *via* partial esterification of the primary hydroxyl groups of the threaded CDs to afford PRX-*g*-PDMS **P1** (**Scheme 3b**, **Scheme S1b**). ^{1}H NMR spectroscopic analysis of **P1** revealed an average of three PDMS chains per PRX (integral ratios of resonances **i'** with **7** and **8**, SI, **Fig. S2**). PRX-*g*-PDMS **P1** was self-assembled using the same process as for **P0** to afford SNPs. The poor solubility of **P1** in common GPC mobile phases (e.g., THF, DMF or

Journal of Materials Chemistry A Accepted Manuscript

H_2O) prevented determination of the molecular weights characteristics via this approach.

3.3 Synthesis of copolymer (PEG-*g*-PDMS, P2)

In order to obtain a direct comparison between PDMS units conjugated on a mobile linker (i.e., CD moieties) and a non-mobile linker, the grafted copolymer PEG-*g*-PDMS **P2** was synthesised. The PDMS acid derivative was covalently conjugated to P(EG-co-Gly) *via* esterification to afford **P2**, whereby the PDMS groups are grafted from the PEG copolymer backbone and fixed in position (**Scheme 3c**, **Scheme S1c**). ^{1}H NMR spectroscopic analysis revealed that both **P1** and **P2** have approximately the same amount of PDMS chains with respect to molecular weight to the polymer backbone (i.e. 6 PDMS grafts per polymer backbone, ESI, **Fig. S2 and 3**).

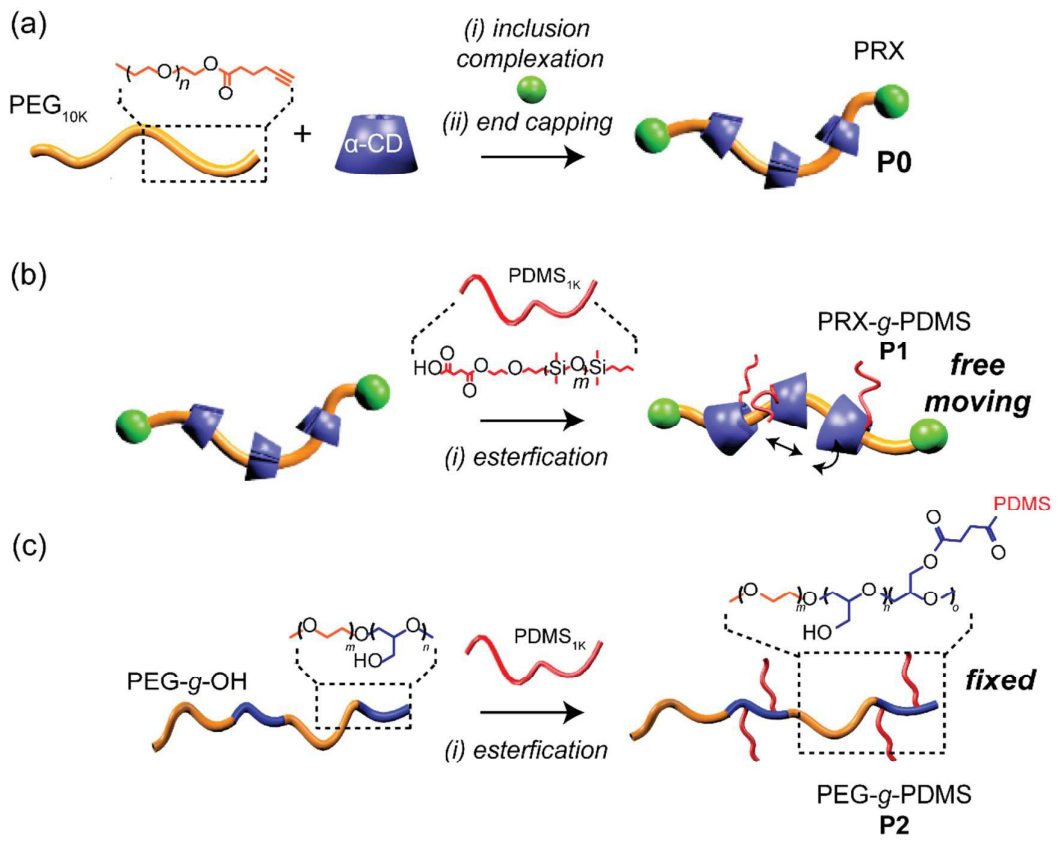

Scheme 3. Synthetic outline showing the prepartion of the SNP precursors **(a)** PRX **P0**, **(b)** PRX-*g*-PDMS **P1** and **(c)** PEG-*g*-PDMS **P2**.

Journal of Materials Chemistry A Accepted Manuscript

3.4 Synthesis of SNPs via self-assembly

The **SNP0**, **SNP1** and **SNP2** were prepared by adding the polymeric precursors **P0**, **P1** and **P2** separately to an IPA:*n*-BuOH mixture (3: 1 vol%) and heated at 40 °C prior to mixing with a Pebax® 2533 solution (IPA:n-BuOH) to generate the selective layer. The appearance of all the polymeric mixtures (0.5 mg/mL) at 25 °C appeared cloudy with the highest opacity observed for the **SNP0** mixture (**Figure 1a**, left). The opacity observed with both **SNP0** and **SNP1** mixtures was attributed to the generation of multi-core micelles whereby the PRXs aggregate *via* intra- and intermolecular hydrogen bonding between threaded CDs (**Figure 1a**). In addition, a lower extent of aggregation was observed for the **SNP1** mixture in comparison to the **SNP0** mixture. This is attributed to the PDMS chains helping to break the hydrogen bonding between the CDs. Dynamic light scattering (DLS) measurements (intensity) recorded at 25 °C further supported the visual observations providing evidence for the formation of aggregates with an average hydrodynamic radius (D_R) = 830 and 930 nm for **SNP0** and **SNP1**, respectively (**Figure 1c-d**, blue traces). Interestingly, when the polymeric mixtures were heated to 40 °C they appeared clear (**Figure 1a**, right). DLS measurements at 40 °C revealed a significant decrease in particle size (**Figure 1c-e**) suggesting disassembly of the multi-core aggregates and the formation of micelles referred to as SNPs. It is hypothesised that the amphiphilic polymers self-assemble into smaller core-shell particles whereby the soluble PEG components form a shell and the less soluble PDMS components form a core (**Figure 1b**). The dynamic nature of the PRXs **P0** and **P1** allows the CDs to move along the PEG chains towards each other creating a large hydrophobic core. In addition, as the CDs move along the chains bundling together the PEG chains are further exposed to form a stabilising hydrophilic corona (**Figure 1b**, left and centre). Hydrogen bonding between threaded CDs, both inter- and intra-molecularly, is well documented and has been used widely to fabricate physically cross-linked hydrogels.[33] At 40 °C the **P1**-based SNPs were smaller (D_R = 46 nm) than the **P0**-based SNPs (D_R = 51 nm) as determined by DLS measurements (**Figure 1c-d**, red trace). This is attributed to the conjugated hydrophobic PDMS chains which would further drive the self-assembly process and create a more densely aggregated core (**Figure 2b**, left versus centre). In comparison, the size change was less pronounced for **SNP2** when the temperature was increased from 25 to 40 °C (**Figure 1c-e**), which was attributed to the fixed conjugation of the PDMS chains in **P2** restricting further aggregation.

Journal of Materials Chemistry A Accepted Manuscript

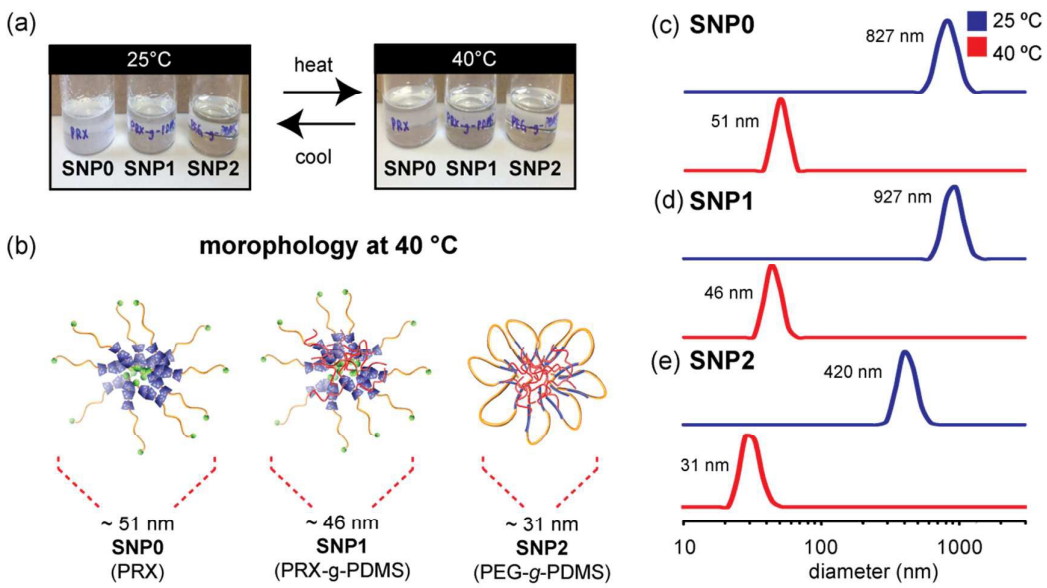

Figure 1. Photographic images of **SNP0**, **SNP1** and **SNP2** mixtures (0.5 mg/mL) at **(a)** 25 °C and 40 °C. **(b)** Graphical illustration of the self-assembled SNPs at 40 °C. **(c-e)** Dynamic light scattering (DLS) measurements of **SNP0**, **SNP1** and **SNP2** mixtures (0.5mg/mL) at 25 °C (blue trace) and 40 °C (red trace). All solutions were self-assembled in an IPA:*n*-BuOH (3:1 vol. %) mixture.

The change in morphology of **P1** when heated from 25 to 40 °C was also investigated using ^{1}H NMR spectroscopy (**Figure 2a** and **b**, respectively). At 25 °C the resonances of the secondary hydroxyl protons of the derivatised α-CDs (**Figure 2a**, resonances 7 and 8) appear ill-defined, which is attributed to hydrogen bonding between CDs limiting segmental movement of the CDs. However, at 40 °C the proton resonances 7 and 8 are better resolved (**Figure 2b**) suggesting a reduction in hydrogen bonding as **P1** rearranges into smaller core-shell micelles.

Journal of Materials Chemistry A Accepted Manuscript

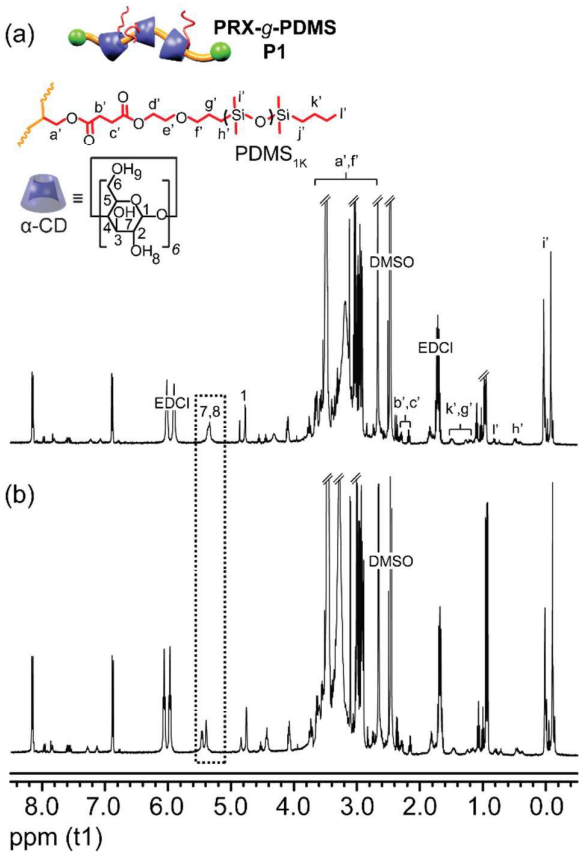

Figure 2. ^{1}H NMR spectra (d_6-DMSO, 400 MHz) of **P1** at **(a)** 25 °C and **(b)** 40 °C.

Journal of Materials Chemistry A Accepted Manuscript

3.5 Membrane preparation and characterization

Commercially available microporous poly(acrylonitrile) (PAN) substrates were chosen as the support material for the TFC membranes as they are resistant to most organic solvents. A solution of diamino terminated PDMS (NH_2-PDMS-NH_2) and trimesoyl chloride (TMC) was spin-coated onto the pre-wetted (H_2O) PAN substrate to form a highly permeable, cross-linked gutter layer (**Scheme 4**). Back filling the PAN substrate with H_2O reduces the noticeable phenomena of pore filling as shown in previous reports.[16, 19] The PDMS intermediate gutter layer prevents the diluted polymer solution penetrating into the microporous PAN substrate during preparation of the selective layer, as well as providing a smoother surface. Solutions containing the additives **SNP0-SNP2** were then mixed with a Pebax® 2533 solution (4 wt. %) at 40 °C and the mixture was spin-coated onto the PDMS gutter layer to afford TFC blend membranes (**Scheme 4**) with various weight percentages (wt%) of SNPs relative to Pebax® 2533. Even though the spin-coating process is at 25°C, the process is rapid (i.e., 40 sec) thus, it is believed that the SNPs retain their micelle conformation. This was further suggested *via* DLS kinetic studies where the SNPs seemed to generally retain their micelle conformation even after 5 min at 25 °C (**Figure S4**).

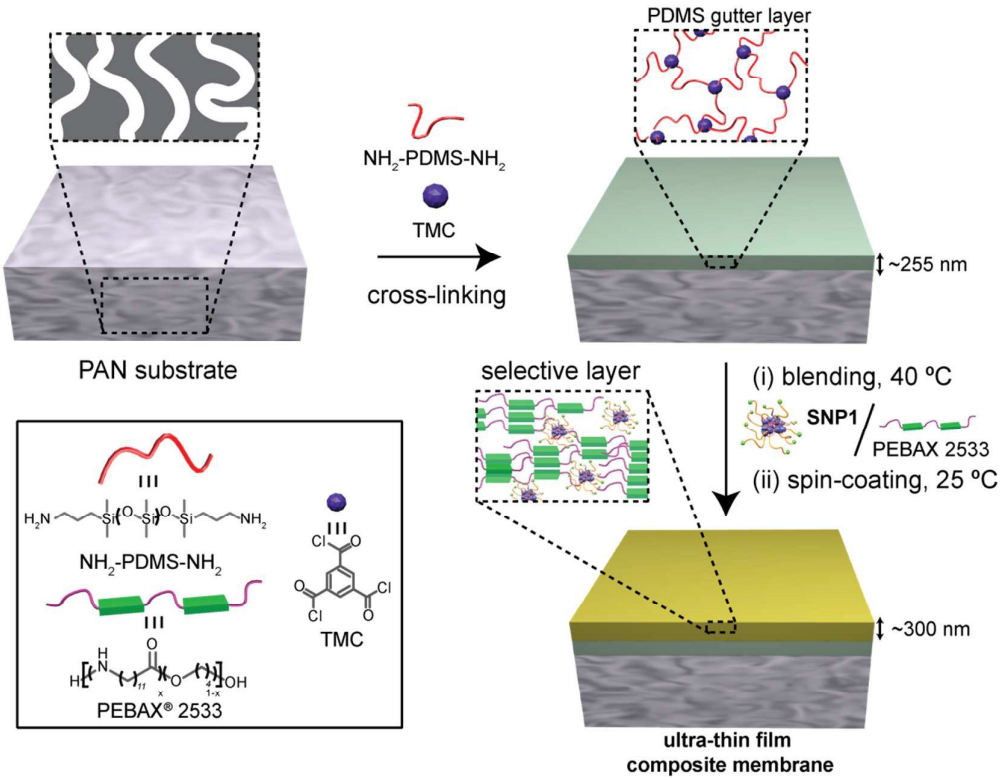

Journal of Materials Chemistry A Accepted Manuscript

Scheme 4. Schematic illustration towards the fabrication of TFC membranes.

The thickness of the PDMS gutter layer was measured by SEM and carried out on a number of different samples. A representative example is presented in **Figure 3a** where the average thickness of the gutter layer was determined to be *ca.* 255 ± 20 nm. To ensure the integrity of the newly formed gutter layer the gas transport properties were measured using the previously described CPVV apparatus (**Scheme 1**). The average CO_2 permeance was 3,000 ± 300 GPU and the average CO_2/N_2 selectivity was 9.0 ± 0.5, which is in good agreement with previously published data.[32] The selective layer was then prepared by spin-coating a mixture of Pebax® 2533 and the additives onto the PDMS gutter layer to afford the TFC membranes. The cross-sectional morphology of the TFC membranes was observed by SEM (**Figure 3b**). The thickness of the selective layer was calculated by subtracting the thickness of the PDMS gutter layer (**Figure 3a**) and was estimated to be *ca.* 300 ± 20 nm in all cases.

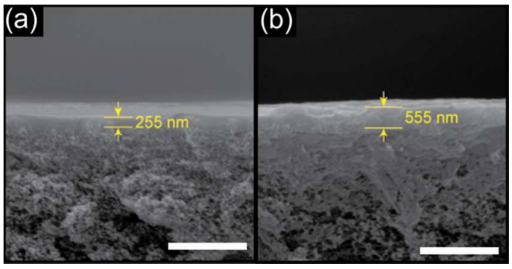

Figure 3. SEM images of the cross-section of the membranes; **(a)** microporous PAN support and the PDMS gutter layer and **(b)** the TFC membrane with Pebax/**P1**-15wt%. Scale bars are 2 μm.

As the crystallinity of additives is known to affect membrane performance, X-ray diffraction (XRD) measurements were performed on the PRX-based polymers **P0** and **P1**, and their respective TFC membranes. Generally, pure Pebax® based materials are crystalline in nature. The XRD pattern obtained from the pure Pebax® 2533 membrane shows three crystalline peaks which are attributed to the crystallisation of the polyamide (2Θ = 22.7 °) and polyether (2Θ = 17.8 and 25.9 °) segments, respectively (**Figure 4a**). Additionally, owing to the hydrogen bonding between threaded CDs, PRX-based materials are also crystalline in nature.[23, 34] This phenomena was further confirmed *via* XRD measurements of the PRX **P0** which revealed typical peaks corresponding to the crystallinity of the PEG units (2θ = 19.1° and 23.3°, **Figure 4b**) and

Journal of Materials Chemistry A Accepted Manuscript

also a crystalline peak attributed to inclusion complexation (2θ = 19.7°, **Figure 4b**).[35] When PDMS chains are conjugated onto the CDs, as in PRX **P1**, the crystalline peaks associated with inclusion complexation disappear (**Figure 4b** and **d**). The disappearance of this peak is attributed to the amorphous PDMS side chains breaking the hydrogen bonding between CDs. The XRD patterns of the TFC blend membranes (Pebax®/**SNP0**-15wt% and Pebax®/**SNP1**-15wt%) revealed a new crystalline peak (2θ =16.9°, **Figure 4b** and **e**, respectively) which is suggestively attributed to the self-assembly of **P0** and **P1** in the membranes. Furthermore, no peaks associated with PRX crystallisation were observed, indicating favourable intermixing, well dispersed SNPs, and a strong interaction between the PRX-based SNP additives and the Pebax® matrix.

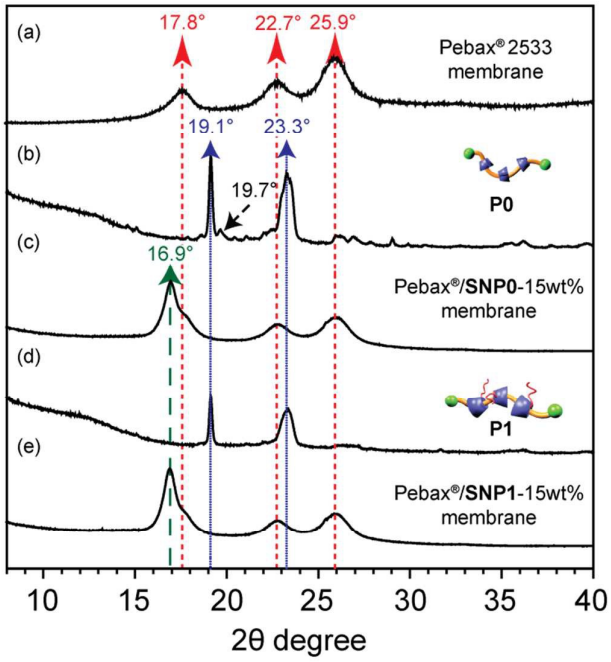

Figure 4. X-ray diffraction (XRD) patterns of **(a)** Pebax® 2533 membrane **(b) P0**, **(c)** Pebax®/**SNP0**-15wt% TFC membrane, **(d) P1** and **(e)** Pebax®/**SNP1**-15wt% TFC membrane.

3.6 Gas transport properties

The ability of the TFC membranes to selectively separate CO_2 from N_2 was studied using an in-house built CPVV apparatus (**Scheme S1**). A minimum of three membranes for each type and wt% of SNP additive were prepared and good reproducibility was obtained.

Journal of Materials Chemistry A Accepted Manuscript

The CO_2 permeance and CO_2/N_2 selectivity for the TFC membranes with varying wt% of **SNP1** relative to Pebax® 2533 were determined at 35 °C and a feed pressure of 340 kPa (**Figure 5**). An increase in CO_2 permeance was observed with increasing wt% of **SNP1**, suggesting that the SNPs (*via* the self-assembly of **P1**) are responsible for increasing the gas permeance through the TFC membranes. The significant increase in flux is believed to be attributed to three individual effects; (i) the increased concentration of ethylene glycol units which increases CO_2 selectivity[17], (ii) the bulky architecture of the SNPs which increases the fractional free volume (FFV) and hence increase CO_2 diffusivity and (iii) the homogenous dispersion of the SNPs increasing the inter-chain distance (*d*-space).[16] It is often difficult to determine the FFV of TFC membranes as the polymeric layer is substantially thinner than the porous substrate. However, density experiments on the dense membrane equivalents confirm that the FFV of the corresponding membranes increases by addition of SNPs (**Figure S5**). This phenomenon has also been seen in the literature were the addition of PEG-based additives increased the FFV of dense and thin film membranes.[36, 37]

The Pebax®/**SNP1**-15wt% TFC membranes displayed approximately a 2.6 fold increase in CO_2 permeance relative to membranes with no additives (**Table 1**, Entry 4 and 1, respectively), whilst maintaining a constant CO_2/N_2 selectivity of approximately 20 (**Figure 5b**). A decrease in the CO_2/N_2 selectivity (< 20) was observed when the loading of **SNP1** was increased > 15 wt% (**Figure 5b**). Therefore, in order to fabricate TFC membranes with desirable separation performance, the optimal amount of **SNP1** added is 15 wt%.

A trade-off plot of CO_2/N_2 selectivity versus CO_2 permeance is shown in **Figure 5c**, which also includes the target performance area[38] for economical post combustion capture by membrane processes. The target area for optimal membrane performance requires a CO_2 permeance ≥ 1,000 GPU (1 GPU = 10^{-6} cm^3(STP) cm^{-2} s^{-1} $cmHg^{-1}$) and a CO_2/N_2 selectivity between 20 and 100. TFC membranes with 15 wt% **SNP1** displayed separation performance within the target region (**Figure 5c**) and superior performance relative to conventional cellulose acetate (CO_2 permeance ~ 100 GPU, CO_2/N_2 selectivity ~ 30)[38] and pure Pebax® 2533 membranes (**Table 1**, Entry 1).

Journal of Materials Chemistry A Accepted Manuscript

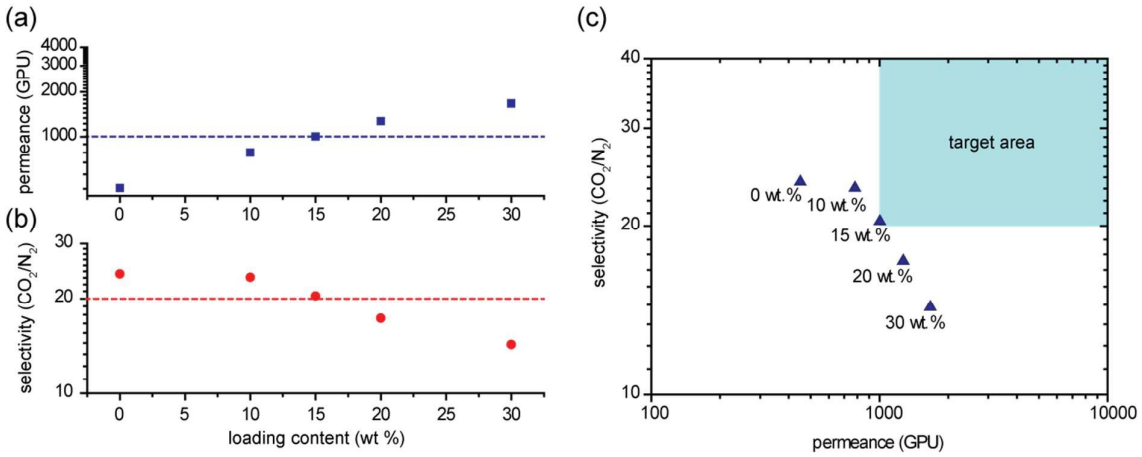

Figure 5. (a) CO_2 permeance and **(b)** CO_2/N_2 selectivity of the TFC membranes as a function of **P1** content (wt% relative to Pebax®) determined at 35 °C and 340 kPa. **(c)** Trade-off plot between CO_2/N_2 selectivity and CO_2 permeance for Pebax® and Pebax®/**SNP1** TFC membranes. The target area is that proposed by Merkel *et al*.[38]

As the gas permeation through the selective layer of TFC membranes reveals the true potential of the membrane materials, the performance of the selective layer was calculated using the sum of resistance model considering the resistance of the gutter layer and the selective layer,[13, 15, 32] and is shown in **Table S1** and **Figure S6**. Pebax®/**SNP1** TFC membranes with 10, 15 and 20 wt% **SNP1** displayed theoretical CO_2 permeances > 1,000 GPU and CO_2/N_2 selectivities > 20 for their selective layers (**Figure 5c**). All of these TFC membranes fell within the target performance area and demonstrate the potential for PRX-based additives to be economically viable for CO_2 capture applications with improvements (decreasing thickness) to the gutter and substrate layers.

Table 1. Gas separation performance of the TFC membranes studied at 35 °C and 340 kPa.

Entry	Sample code	Additive (wt%)	TFC Membrane	
			J (CO_2)[a] (GPU)	CO_2/N_2 Selectivity
1	Pebax®	0	385	24
2	Pebax®/**SNP0**-15wt%	15	596	24
3	Pebax®/**SNP1**-10wt%	10	782	23

Journal of Materials Chemistry A Accepted Manuscript

4	Pebax®/**SNP1**-15 wt%	15	1,000	20
5	Pebax®/**SNP1**-20 wt%	20	1,270	17
6	Pebax®/**SNP1**-30 wt%	30	1,670	14
7	Pebax®/**SNP2**-15 wt%	15	681	15
8	Pebax®/**CD**-15 wt%	15	468	10
9	Pebax®/**PDMS**-15 wt%	15	1,310	15

[a] CO_2 permeance.
[b] CO_2 permeability. 1 Barrer = 1 x 10^{-10} cm^3(STP)·cm ·cm^{-2}·s^{-1}·$cmHg^{-1}$.

The thicknesses of the selective layers (*ca.* 280-320 nm), as estimated from SEM images, were used in conjunction with mass transport theory equations to calculate the CO_2 permeability of the selective layers (**Table S1**). By increasing the **SNP1** mass fraction to 30 wt%, the CO_2 permeability of the selective layer could be enhanced approximately six-fold, while still maintaining a selectivity of ~ 20, when compared to a pure Pebax® 2533 selective layer (**Table S1**, Entry 6 and Entry 1, respectively). This trend of increasing permeability without a significant drop in selectivity corresponds to the previously reported series model,[39] which is highly desirable. The ability to achieve this using PRX-based technology as SNP additives highlights their potential as candidates for novel gas separation membranes.

Owing to the dynamic nature of threaded CDs within PRXs, it was anticipated that TFC membranes prepared with PRX additive **SNP1** would display significantly different gas transport properties compared to conventional additives such as **SNP2**, where the PDMS chains are fixed permanently. A comparison of gas separation performance of the Pebax®/**SNP1**-15wt% TFC membrane versus the Pebax®/**SNP2**-15wt% TFC membrane and other previously reported polymeric TFC membranes with the same additive loading (15 wt%) is shown in **Figure 6**. The target area based on the economics of gas separation in post-combustion capture is also included. In comparison with the pure Pebax® 2533 TFC membrane (**Figure 6**, green circle) and other TFC membranes (**Figure 6**, 1-8, open circles), the Pebax®/**SNP1**-15wt% TFC membrane (**Figure 6a**, red star) reaches a high CO_2 permeance (1,000 GPU) with a reasonable CO_2/N_2 selectivity (20). The only more permeable TFC membrane (**Figure 6**, 8, PDMS) displays a lower

Journal of Materials Chemistry A Accepted Manuscript

CO_2/N_2 selectivity of 15, which is unlikely to be selective enough, regardless of the permeance. When specifically comparing TFC membranes with dynamic additives (i.e., **SNP1**) and fixed additives (i.e., **SNP2**), the Pebax®/**SNP1**-15wt% TFC membrane exhibited ~ 1.5 fold increase in permeance and ~ 2 fold increase in selectivity (**Figure 6**, red star versus 6, and **Table 1**, entry 2 versus 7). These interesting results suggest that freely moving PDMS chains within confined areas of TFC membranes play an important role in increasing gas transport properties. This phenomena is attributed to the mobility of CD conjugated PDMS chains leading to two combinatory factors upon self-assembly; the further exposure of the CO_2-phillic PEG backbone and the larger core when compared to covalent analogous **SNP2** resulting in higher permeability. The ability to achieve gas performance targets at lower additive consumptions relative to current methods in the literature[13, 19] makes the Pebax/**SNP1**-15 wt% TFC membrane an economically attractive candidate for efficient CO_2 separation applications.

The SNP TFC system (**Figure 6**, star icon) was also compared with commercial membrane systems (**Figure 6**, purple triangle)[38] and polymers of intrinsic microporosity (PIM) based membranes (**Figure 6**, orange triangle); a recent strategy which has produced high gas separation performance. The SNP TFC membrane exhibited a higher permeance when compared to both commercial membranes (permeance ~100, selectivity ~50) and the PIM based membranes (permeance ~80 GPU, selectivity ~30).[7] Although PIM based membranes show high CO_2 permeability (~3000 barrer),[7] they are operationally difficult to control due to the inability to form thinner membranes. The higher permeance seen with the **SNP1** TFC system is attributed to the ability to form substantially thinner membranes (i.e., selective layer ≤ 1 μm) allowing for increased flux.

Journal of Materials Chemistry A Accepted Manuscript

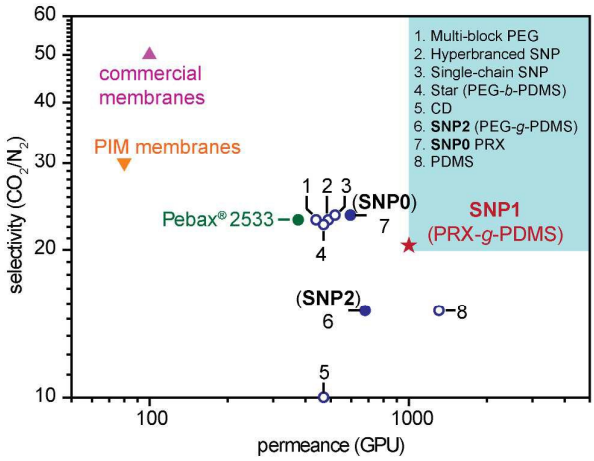

Figure 6. CO_2/N_2 selectivity versus CO_2 permeance plot comparing the performance of Pebax®/**SNP1**-15wt% TFC membrane (star icon) with **(a)** previously reported TFC membranes 1-8 at the same additive loading (15 wt%). Entries 1-4 are TFC membranes reported by our group [10, 12, 13], while entries 5-8 are TFC membranes prepared in this study. The blue box is the target area proposed by Merkel *et al*. [33].

To further understand this novel system, single gas (CO_2 and N_2) permeation measurements were conducted on the TFC membranes across a range of feed pressures at 35 °C. **Figure 7** presents the CO_2 permeance and CO_2/N_2 selectivity as a function of the feed gas pressure. With increasing feed pressure, pure Pebax® 2533, Pebax® /**SNP0**-15wt% and Pebax® /**SNP2**-15wt% TFC membranes showed an increase in CO_2 permeance (**Figure 7a**, square, circle and diamond symbols, respectively) and a decrease in CO_2/N_2 selectivity (**Figure 7b**). This trend is generally reported in the literature and can be attributed to CO_2-induced plasticization.[40] Plasticization occurs when CO_2 molecules causes the polymer matrix to swell, leading to increased FFV, and increased gas diffusivity. This results in a reduction in CO_2/N_2 selectivity as the change in diffusivity is greater for the lighter gas molecules (i.e., N_2). Interestingly, the Pebax®/**SNP1**-15wt% TFC membrane showed a divergent trend where a decrease in CO_2 permeance (*ca.* 140 GPU) was seen when the feed pressure increased to 900 kPa (**Figure 7a**, triangle symbols). This phenomenon may be attributed to the dynamic nature of the SNPs, which may be compacted at high pressures and leading to a reduction in FFV. This results in decreased permeance of both CO_2 and N_2 with increasing feed pressure.

Journal of Materials Chemistry A Accepted Manuscript

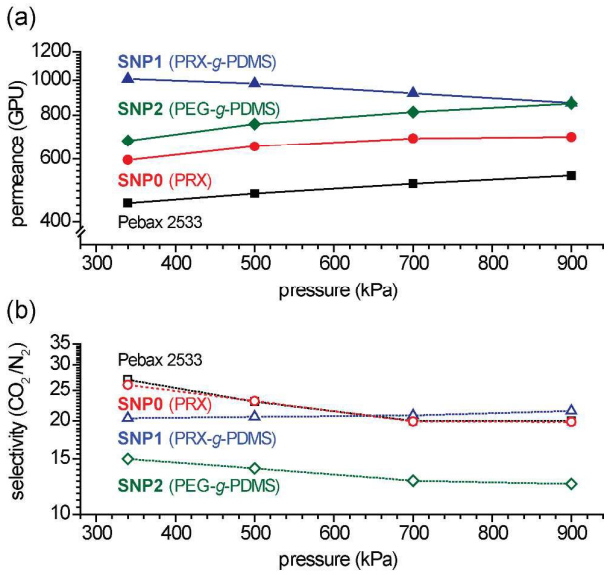

Figure 7. (a) CO_2 permeance and **(b)** CO_2/N_2 selectivity of pure Pebax® 2533 (squares), Pebax®/**SNP0**-15wt% (circles), Pebax®/**SNP2**-15wt% (diamonds) and Pebax®/**SNP1**-15wt% (triangles) TFC membranes as a function of feed pressure at 35 °C.

The effect of operating temperature on membrane performance was also investigated using a temperature range of 25-45 °C at a constant feed pressure of 340 kPa. The CO_2 permeance and CO_2/N_2 selectivity of TFC membranes versus temperature is shown in **Figure 8**. Higher temperatures are known to enhance gas permeance due to an increase in polymer chain mobility leading to increased gas diffusivity.[41] This trend was observed for all of the TFC membranes, where the CO_2 permeance increased by ~ 80, 130, 210 and 210 GPU in pure Pebax® 2533, Pebax®/**SNP0-**15wt%, Pebax®/**SNP1**-15wt% and Pebax®/**SNP2**-15wt% TFC membranes, respectively, when the operating temperature was increased from 25 to 45 °C. This phenomenon is also typical for non-porous polymeric membranes as higher gas flux is recorded with higher temperatures.[42] Although the CO_2 permeance was enhanced at high operating temperatures, the CO_2/N_2 selectivity of all of the TFC membranes decreased at 45 °C, with the exception of the Pebax®/**SNP1**-15wt% TFC membrane (**Figure 8b**). The reduction in CO_2/N_2 selectivity can be attributed to N_2 diffusivity increasing at a greater rate than CO_2. This trend has also been commonly observed in the literature.[36]

Journal of Materials Chemistry A Accepted Manuscript

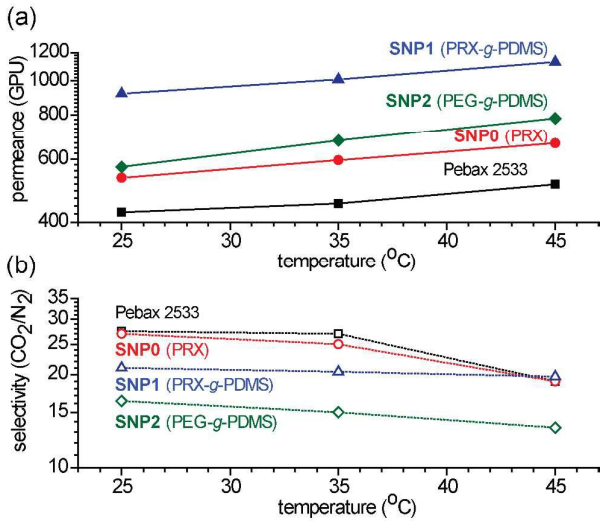

Figure 8. (a) CO_2 permeance and **(b)** CO_2/N_2 selectivity of the Pebax® 2533 (squares), Pebax®/**SNP0**-15wt% (circles), Pebax®/**SNP1**-15wt% (triangles) and Pebax®/**SNP2**-15wt% (diamonds) TFC membrane as a function of temperature at 340 kPa.

4. Conclusion

In summary, we report the preparation of PRX-based TFC membranes for CO_2/N_2 separation applications for the first time. Using CD/PEG PRXs as the building blocks, PDMS chains were conjugated onto the CD units and displayed translational and rotation freedom. The dynamic nature of this system allowed the self-assembly of PRX-based graft copolymers into SNPs. The supramolecular SNPs were subsequently utilized as additives in the Pebax® selective layer of TFC membranes. It was shown that the CO_2 permeance of TFC membranes could be significantly increased whist maintaining good CO_2/N_2 selectivities. The ability of the PRX-based TFC membranes to separate CO_2 from N_2 was studied at various temperatures (25-45 °C) and pressures (340-900 kPa). The highest CO_2 permeance with reasonable CO_2/N_2 selectivity was found in TFC membranes containing 15 wt% additive. The low mass fraction needed to achieve commercially viable gas transport properties makes these membranes highly desirable for large scale capture applications. The increased CO_2 permeance was attributed to the increase in CO_2-philic characteristics as a result of the dynamic nature of the SNP additives, and the increase in FFV due to the increase in Pebax® inter-chain distance. The performance of the Pebax®/**SNP1**-15wt% TFC membrane and its selective layer

Journal of Materials Chemistry A Accepted Manuscript

successfully fell within CO_2 separation performance targets (permeance ≥ 1,000 GPU and CO_2/N_2 selectivity ≥ 20), highlighting the potential of PRX-based TFC membranes for efficient CO_2 separations.

Acknowledgments

The authors acknowledge the funding provided by the Australian Government through the CRC program. The authors also acknowledge the Australian Research Council under the Future Fellowship (FT110100411, G.G.Q.) and the Super Science Fellowship (FS110200025) Schemes.

Author contributions

S.T. and Q.F. designed and performed the experiments. J.K. and J.S. helped to analyse the data. All authors contributed to data analysis and wrote the manuscript. These authors contributed equally (S.T. and Q.F.).

5. References

[1] R. W. Baker, B. T. Low, *Macromolecules* **2014**, *47*, 6999.
[2] C. E. Powell, G. G. Qiao, *Journal of Membrane Science* **2006**, *279*, 1.
[3] Y. Yampolskii, *Macromolecules* **2012**, *45*, 3298.
[4] M. Zhao, A. I. Minett, A. T. Harris, *Energy & Environmental Science* **2013**, *6*, 25.
[5] S. Li, C. Q. Fan, *Industrial & Engineering Chemistry Research* **2010**, *49*, 4399.
[6] J. C. White, P. K. Dutta, K. Shqau, H. Verweij, *Langmuir* **2010**, *26*, 10287.
[7] N. Du, H. B. Park, G. P. Robertson, M. M. Dal-Cin, T. Visser, L. Scoles, M. D. Guiver, *Nat Mater* **2011**, *10*, 372.
[8] W. Yave, A. Car, J. Wind, K.-V. Peinemann, *Nanotechnology* **2010**, *21*, 395301.
[9] S. Li, Z. Wang, X. Yu, J. Wang, S. Wang, *Advanced Materials* **2012**, *24*, 3196.
[10] S. Zhao, Z. Wang, Z. Qiao, X. Wei, C. Zhang, J. Wang, S. Wang, *Journal of Materials Chemistry A* **2013**, *1*, 246.
[11] G. Dong, H. Li, V. Chen, *Journal of Materials Chemistry A* **2013**, *1*, 4610.
[12] T.-H. Bae, J. S. Lee, W. Qiu, W. J. Koros, C. W. Jones, S. Nair, *Angewandte Chemie International Edition* **2010**, *49*, 9863.
[13] A. Halim, Q. Fu, Q. Yong, P. A. Gurr, S. E. Kentish, G. G. Qiao, *Journal of Materials Chemistry A* **2014**, *2*, 4999.
[14] T.-S. Chung, L. Y. Jiang, Y. Li, S. Kulprathipanja, *Progress in Polymer Science* **2007**, *32*, 483.
[15] Q. Fu, A. Halim, J. Kim, J. M. P. Scofield, P. A. Gurr, S. E. Kentish, G. G. Qiao, *Journal of Materials Chemistry A* **2013**, *1*, 13769.

Journal of Materials Chemistry A Accepted Manuscript

[16] Q. Fu, E. H. H. Wong, J. Kim, J. M. P. Scofield, P. A. Gurr, S. E. Kentish, G. G. Qiao, *Journal of Materials Chemistry A* **2014**, *2*, 17751.
[17] S. L. Liu, L. Shao, M. L. Chua, C. H. Lau, H. Wang, S. Quan, *Progress in Polymer Science* **2013**, *38*, 1089.
[18] Q. Wang, Z. Dong, Y. Du, J. F. Kennedy, *Carbohydrate Polymers* **2007**, *69*, 336.
[19] J. M. P. Scofield, P. A. Gurr, J. Kim, Q. Fu, A. Halim, S. E. Kentish, G. G. Qiao, *Journal of Polymer Science Part A: Polymer Chemistry* **2015**, DOI: 10.1002/pola.27628.
[20] F. van de Manakker, T. Vermonden, C. F. van Nostrum, W. E. Hennink, *Biomacromolecules* **2009**, *10*, 3157.
[21] A. Harada, M. Kamachi, *Macromolecules* **1990**, *23*, 2821.
[22] A. Harada, J. Li, M. Kamachi, *Nature* **1992**, *356*, 325.
[23] A. Harada, J. Li, T. Nakamitsu, M. Kamachi, *The Journal of Organic Chemistry* **1993**, *58*, 7524.
[24] Y. Kawaguchi, A. Harada, *Journal of the American Chemical Society* **2000**, *122*, 3797.
[25] S. Tan, K. Ladewig, Q. Fu, A. Blencowe, G. G. Qiao, *Macromolecular Rapid Communications* **2014**, *35*, 1166.
[26] S. Tan, E. H. H. Wong, Q. Fu, J. M. Ren, A. Sulistio, K. Ladewig, A. Blencowe, G. G. Qiao, *Australian Journal of Chemistry* **2014**, *67*, 173.
[27] J. Araki, T. Kataoka, K. Ito, *Soft Matter* **2008**, *4*, 245.
[28] S. Tan, A. Blencowe, K. Ladewig, G. G. Qiao, *Soft Matter* **2013**, *9*, 5239.
[29] S. Tan, E. Nam, J. Cui, C. Xu, Q. Fu, J. M. Ren, E. H. H. Wong, K. Ladewig, F. Caruso, A. Blencowe, G. G. Qiao, *Chemical Communications* **2015**.
[30] J. Zhou, H. Ritter, *Polymer Chemistry* **2010**, *1*, 1552.
[31] Z. Li, P. Li, J. Huang, *Journal of Polymer Science Part A: Polymer Chemistry* **2006**, *44*, 4361.
[32] P. Li, H. Z. Chen, T.-S. Chung, *Journal of Membrane Science* **2013**, *434*, 18.
[33] X. Liao, G. Chen, X. Liu, W. Chen, F. Chen, M. Jiang, *Angewandte Chemie International Edition* **2010**, *49*, 4409.
[34] M. Okada, A. Harada, *Macromolecules* **2003**, *36*, 9701.
[35] Q. Fu, J. M. Ren, G. G. Qiao, *Polymer Chemistry* **2012**, *3*, 343.
[36] A. Car, C. Stropnik, W. Yave, K.-V. Peinemann, *Separation and Purification Technology* **2008**, *62*, 110.
[37] A. Car, C. Stropnik, W. Yave, K.-V. Peinemann, *Journal of Membrane Science* **2008**, *307*, 88.
[38] T. C. Merkel, H. Lin, X. Wei, R. Baker, *Journal of Membrane Science* **2010**, *359*, 126.
[39] L. M. Robeson, *Industrial & Engineering Chemistry Research* **2010**, *49*, 11859.
[40] A. Bos, I. G. M. Pünt, M. Wessling, H. Strathmann, *Journal of Membrane Science* **1999**, *155*, 67.
[41] S. Kelman, H. Lin, E. S. Sanders, B. D. Freeman, *J. Membr. Sci.* **2007**, *305*, 57.
[42] L. Liu, A. Chakma, X. Feng, *Ind. Eng. Chem. Res.* **2005**, *44*, 6874.

Journal of Materials Chemistry A Accepted Manuscript